Energy Reports 11 (2024) 71–82

Contents lists available at ScienceDirect

Energy Reports

journal homepage: www.elsevier.com/locate/egyr

Research paper

Feasibility study on energy harvesting with thermoelectric generators in a photovoltaic-ground source heat pump system

Hobyung Chae [a,*], Sangmu Bae [a], Jae-Weon Jeong [c], Yujin Nam [b]

[a] Research Institute of Industrial Technology, Pusan National University, Busan 46241, South Korea
[b] Department of Architectural Engineering, Pusan National University, Busan 46241, South Korea
[c] Department of Architectural Engineering, College of Engineering, Hanyang University, Seoul 04763, South Korea

ARTICLE INFO

Keywords:
Thermoelectric generator
Energy harvesting
Feasibility study
Hybrid system
Generated electricity

ABSTRACT

Thermoelectric generators (TEGs) harness temperature differences to produce electricity and hold promise for diverse industrial applications. However, their limited conversion efficiency casts doubt on their role in achieving energy independence. This study introduces an advanced technique that exploits temperature gradients in water pipes, utilizing supplementary TEGs to augment power generation. This method maintains a stable temperature gradient for TEG operation. Additionally, TEG power output can be efficiently modulated via flow control. In the feasibility evaluation for residential settings, the temperature fluctuations across each system unit were analyzed. In the active system, the chosen sites for TEG integration were units equipped to manage heat transfer using working fluids. The inlet and outlet temperatures were calculated for photovoltaic-thermal (PVT) systems, ground heat exchangers (GHEs), and heat storage tanks (HSTs). The electricity produced by the TEGs was benchmarked against their conversion efficiency, zT. The results indicated that the TEGs yielded 10.95 kWh of electricity when systematically implemented in each unit. To realize a zero-energy building, an area of 64.5 m^2 per unit is necessitated for TEG deployment, given a zT value of 1.

1. Introduction

Recent increases in energy consumption and carbon emissions have resulted in visible climate change effects, such as rising sea levels and global warming (Campagna and Fiorito, 2022). To address these issues, 195 nations approved the Paris Agreement on Climate Change, agreeing to establish their own greenhouse gas reduction targets, and to monitor their implementation (Joung et al., 2020; Mavromatidis et al., 2016). National policies and R&D support initiatives have been undertaken, aiming to decrease energy consumption in the construction industry, considering that this accounts for 36% of total energy consumption and 39% of greenhouse gas emissions (Song and Kim, 2022; Hamilton and Rapf, 2020). To decrease energy usage in the construction industry, it is critical to employ a high-efficiency 'active system' based on renewable energy alongside a 'passive system' based on high insulation and airtight materials. Efforts are ongoing to create zero-energy buildings (ZEBs) which use heat pump and photovoltaic (PV) systems based on passive systems that decrease heat loss in many cases (Omrany et al., 2022; Ahmed et al., 2022; Marszal et al., 2011). However, since it is difficult to secure a PV installation area and to receive adequate solar radiation in a limited urban space, PV systems are restricted in their ability to manage the power consumption of entire buildings. In particular, achieving the ZEBs and carbon neutrality requires research into additional electricity production system and heat recovery technologies.

Heat recovery systems play a pivotal role in enhancing energy efficiency across industries and utilities. By capturing and repurposing waste heat, these systems not only reduce operational costs but also diminish environmental impact through lowered greenhouse gas emissions. Their implementation not only prolongs equipment lifespan but also optimizes overall process efficiency. Khan et al (Khan et al., 2020a, 2020b). introduced a conceptual design for a power generation system, leveraging both a 400 MWth lead-based reactor with high performance and a 10 MWth lead-based reactor. Their design approach utilized mathematical and numerical methodologies. A representative heat recovery system in residential buildings is tge energy recovery ventilator utilizing the supply and return air for heating and cooling. Typically, the systems can attain a sensible heat recovery rate ranging from 50% to 80% (Sammeta et al., 2011). Heat transfer efficiency in heat recovery is influenced by factors such as plate constructions (Khan et al., 2010), heat exchanger materials (Nasif et al., 2010; Lu et al., 2010), and flow patterns (Gherasim et al., 2011).

* Corresponding author.
E-mail address: namyujin@pusan.ac.kr (H. Chae).

https://doi.org/10.1016/j.egyr.2023.11.023
Received 18 August 2023; Received in revised form 26 September 2023; Accepted 9 November 2023
Available online 25 November 2023

Nomenclature

A	Area [m^2]
C_p	Volumetric heat capacity [$kJ/(m^3 \bullet K)$]
G	Beam and diffuse radiation incident on the PV cell surface [W/m^2]
$X_{celltemp}$	Multiplier for the power efficiency as a function of the PV cell temperature [1/K]
$X_{radiation}$	Multiplier for the power efficiency as a function of the incident radiation [m^2/W]
I	Electrical current in circuit [C/s]
J	Current density [A/m^2]
IAM	Incidence angle modifier [%]
L	Length [m]
$\dot{m}$	Flow rate [L/min]
N	Number of connected thermocouples [−]
P	Electric output [W]
Q	Thermal energy [kW]
Q_p	The rate of heat absorbed or emitted at either of the two junctions in the circuit [kW]
Q_J	Heat flux by Joule effect [kW]
R	Thermal resistance [K/W]
T	Temperature [℃]
V	Voltage [V]

Greek letters

α	Seebeck coefficient [V/℃]
π	Peltier coefficient [J/C]
ρ	Electrical resistivity of materials [$\Omega \bullet m$]
μ	Thomson coefficient [V/K]
σ	Electric conductivity [1/Ω]
λ	Thermal conductivity [$W/(m \bullet K)$]
ε	Emissivity on PVT surface [-]
τa	Transmittance–absorbance production of PVT [-]
θ	*Angle of incidence [°]*

Subscripts

c	cold side
con	conductor
GHE	Ground heat exchanger
h	hot side
HP	Heat pump
n	N type material
out	outlet
p	P type material
pn	thermocouple
PVT	Photovoltaic-thermal
TEG	thermoelectric generator

Thermoelectric materials allow thermal energy to be converted directly into electrical energy, and electrical energy to be converted directly into thermal energy. The materials and technology of thermoelectric elements are highly suited to current building energy-harvesting demands (Wang et al., 2013; Matiko et al., 2014; Vasiliev et al., 2019). Despite their poor energy conversion efficiency, thermoelectric elements can generate electricity without the need for sophisticated components, unlike traditional heat engines. Furthermore, as material knowledge and analysis have progressed, it has become increasingly feasible to forecast the properties of compounds, and some nano-processing technologies have considerably boosted thermoelectric efficiency alongside the development of thermoelectric elements (Li et al., 2022; Zhao et al., 2016; Boulanger, 2010; Chung et al., 2004). Energy harvesting using thermoelectric elements is gradually emerging as a highly efficient power generation technology, which does not emit CO_2 from fossil fuel combustion, and can be used to generate electricity from low temperature heat sources.

Thermoelectric generators (TEGs) based on thermoelectric elements are used in a variety of industries, and the development and optimization of wearable applications for TEGs that can be driven by human body temperature has even been proposed (Thielen et al., 2017; Proto et al., 2018). Furthermore, wireless sensors self-powered by energy harvesting are being developed for efficient and safe operation in industrial sites. This has the potential to significantly reduce the manpower and maintenance costs associated with battery replacement (Kim et al., 2018; Guan et al., 2017; Iezzi et al., 2017). Furthermore, research is being conducted in the automotive and aerospace industries on the development of applications for power supplies using TEGs (Liu et al., 2016; Zhang et al., 2015; Liu et al., 2018, 2017).

Researchers attempt to develop applications using thermoelectric devices for energy harvesting in the building section. Ko and Jeong (Ko and Jeong, 2021) assessed the yearly power production performances of a building-integrated solar system utilizing a device integrating a PCM and a TEG. Byon and Jeong (Byon and Jeong, 2020) proposed a thermoelectric power production block for use in building envelopes. TEGs combined with a phase change material (PCM) are used in energy harvesting. The difference between the outdoor temperature and the thermoelectric power generation block with the PCM applied to the back-sheet of the TEG by solar radiation and external temperature may be used to examine the efficiency of electricity generation. Thus, energy can be created independently of season or time by utilizing waste heat stored and discharged by the PCM. Furthermore, since the system may be expanded by connecting blocks, it is feasible to construct systems based on power consumption. Despite the new challenges using the TEGs are critical for achieving the ZEBs, it is the limitations to supply sufficient power for building heating and cooling systems due to low electric generation at present. Indeed, the ongoing technological advancements in thermoelectric materials are anticipated to yield greater energy recovery potential. Consequently, it is imperative to undertake a comprehensive feasibility assessment concerning the integration and advancement of TEG applications, with a particular focus on their implementation within active building systems.

In this study, the feasibility of TEG application in each system unit is investigated for houses using the hybrid system. The proposed technology harnesses temperature differences in pipes by employing supplemental TEG application to facilitate power generation. Suitable for various settings with water pipes, this approach ensures a safe temperature gradient for TEG applications. Furthermore, the power output from the TEG can be predicted through flow regulation. The active system in the house consists of a ground source heat pump (GSHP), a photovoltaic-thermal (PVT) system, and a hot storage tank (HST). The systems provide the heat pump with high-potential heat sources, which are output temperatures of either ground heat exchangers (GHE) or PVT through operational control. Thermoelectric applications are located at the inlet and outlet of each system, where the largest temperature difference occurs. The electric generations of the TEG are calculated by the temperature difference according to the operation of each system. Additionally, the electric generations of TEG are compared based on conversion efficiency (zT), and the required installation areas of the TEG applications are analyzed to achieve ZEB.

2. Overview of building systems

Fig. 1 shows a conceptual diagram of the hybrid system used in this

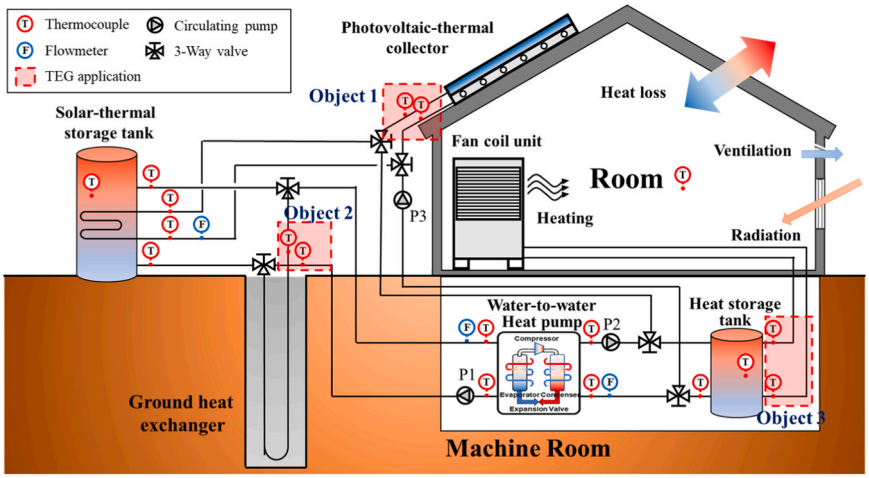

Fig. 1. Schematic diagram of hybrid system.

study. The hybrid system for residential houses consisted of the PVT, the GHE, and the HST units, alongside a water-to-water heat pump, with supplementary heating and cooling provided by a fan coil unit. The thermal energy collected by PVT and GHE was utilized to heat buildings using a heat pump in the application system, whilst the electricity generated by the PVT was supplied to the heat pump power. Furthermore, efficient functioning was possible as well as the ability to adjust to energy demand by using the HST and a solar storage tank (SST). The dynamic energy model using Trnsys 18 was validated by comparing and analyzing results and experimental data from a previous study (Bae and Nam, 2021). The parameters of model units are shown in Table 1.

Fig. 2 shows the system's flow chart, which includes the heating and heat storage operations. Heating was activated during the heating operating time, when the interior temperature fell below 22 °C. At this point, the HST controlled the temperature of the water delivered into the room, whilst circulating water of 42 °C or greater was provided to the fan coil unit to conduct heating. Heat storage utilizing a PVT collector took priority for heat storage in the HST. Heat storage utilizing the PVT continued if the PVT water outlet temperature was 2 °C higher than the HST internal temperature. Otherwise, if the temperature of the PVT's water outlet was greater than the internal temperature of the SST, the heat storage operation in the SST was initiated. The heat pump was then turned on by choosing the highest heat source from the SST and GHX, based on their outlet temperatures. Objects 1–3 in Fig. 2 represent TEGs installed in each unit. The inlet and outlet temperatures of the fluid are calculated for each unit: Object 1 (PVT), Object 2 (GHE), and Object 3 (HST). Table 2 indicates the temperature rage in each object.

Table 1
Parameters of model units.

Unit		Input value	Specification
Heat pump		10.5 kW	Water to water type
PVT collector	Size	1.012 m × 19.72 m	
	Electrical efficiency	16%	
Ground heat exchanger	Depth	200 m	Vertical close-loop type
	Number of boreholes	1	
	Pipe sizes	External diameter: 40 mm, Inside diameter: 32 mm	
Circulating pump	Flow rate	30 L/min	
	Electric consumption	0.2 kW	
Fan coil unit	Heating capacity	23.25 kW	

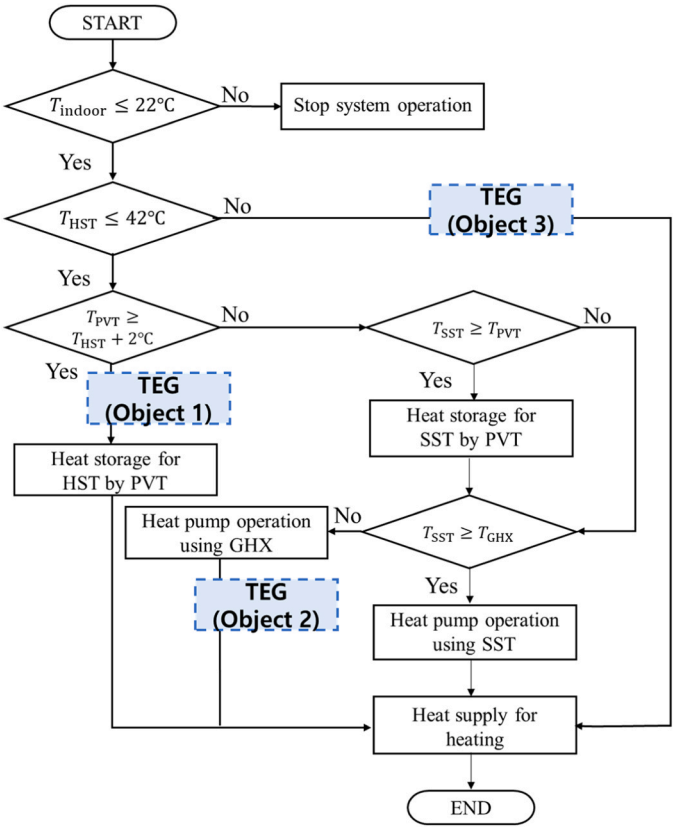

Fig. 2. Flow chart for system operation.

Table 2
Temperature range in each object.

Object	Outlet temperature range (°C)	Inlet temperature range (°C)	Range of temperature difference (°C)
PVT	5.3–40.2	-20.7–40.1	0.0–30.5
GHX	4.2–20.0	8.3–16.83	0.0–10.5
HST	24.2–52.3	20.0–47.0	0.0–15.0

Fig. 3 shows a conceptual diagram of the TEG application. The application structured an angular pipe in a square shape to facilitate TEG contact. The thermoelectric materials were located between the inlet

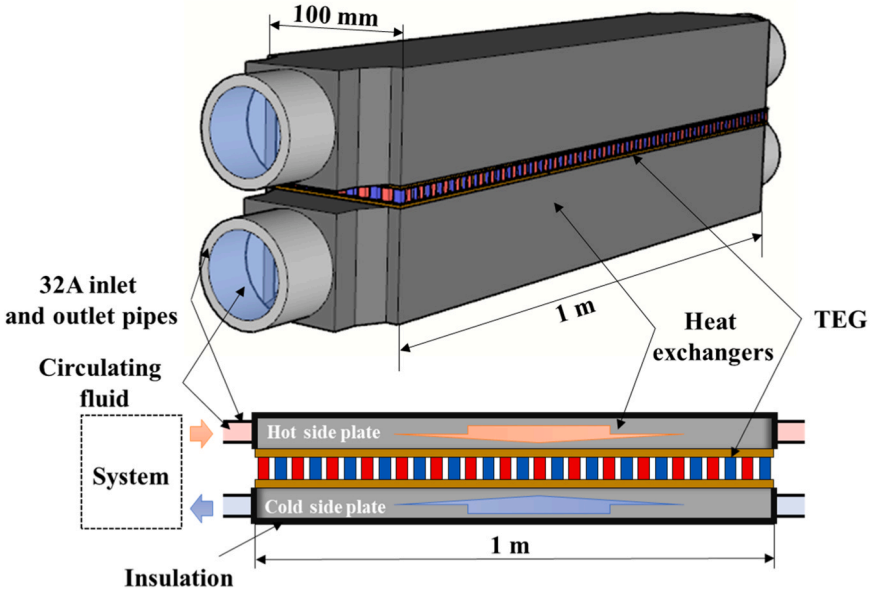

Fig. 3. Conceptual image of TEG application located in pipes.

and outlet pipes. In this manner, a desired temperature difference could be set via flow control, and the electric power produced by the TEG could be estimated. The size of a TEG application is 0.1 m × 1 m, and it is assumed to be insulated except for the sides that are in contact with the TEG materials. The temperature ranges at the inlet and outlet of each system were 0–43℃ (PVT), 7–15℃ (GHE), 40–48℃ (HST) during system operation. The detailed operating temperature ranges and temperature differences of each unit are discussed in the results presented in Chapter 4. Based on these temperatures, the electric power of the TEG is calculated (Chapter 5).

3. Methodology

3.1. Thermoelectric effects

Thermoelectric generators (TEGs) have various advantages, including design simplicity, long-lasting lives, few maintenance requirements, and environmental sustainability. To increase the output of a TEG, multiple thermocouples (TCs) are typically connected in series and parallel. TCs are made of two different materials using the Seebeck coefficient (P-type leg and N-type leg), with their ends being joined with a conductor. TEGs convert thermal energy into electrical energy based on the Seebeck effect. The Seebeck effect, as well as the Peltier, Thomson, and Joule effects, are all influenced by the phenomenon caused by electrical flow and temperature differences. Thus, the axial force should be modeled by considering all of these effects. Fig. 4.

When there is a temperature difference between two junctions, the Seebeck effect produces a voltage in a circuit consisting of two different metals. The voltage generated here is proportional to the temperature difference between the two junctions, whilst the proportionality constant is the Seebeck coefficient, an inherent property of the circuit. At a given temperature difference, the TEG's output voltage Vout can be expressed as follows:

$$V_{\text{out}} = \alpha_{\text{pn}} \Delta T = N\left(\alpha_{\text{p}} - \alpha_{\text{n}}\right)\left(T_{\text{h}} - T_{\text{c}}\right) \tag{1}$$

where α_{p} and α_{n} are the Seebeck coefficient of P- and N-type materials; α_{pn} is the Seebeck coefficient of the TC; T_{h} and T_{c} are the surface temperatures on the hot and cold side plates, and N is the number of ther-

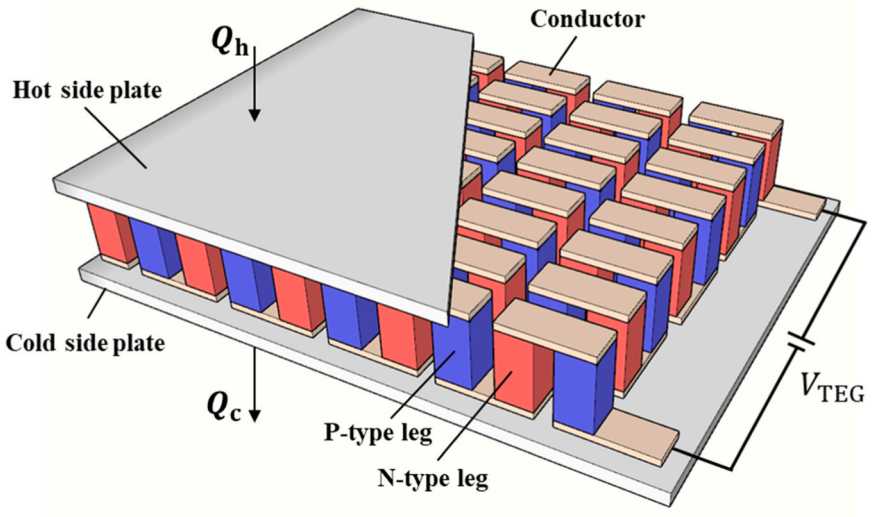

Fig. 4. Schematic overview of thermoelectric generator.

mocouples.

When current flows through a circuit made of two distinct materials, a temperature difference between the two junctions arises. The heating effect of an electric current at the junction of two different metals is defined by the Peltier effect, whilst the I direction of the current determines the junction's heat dissipation or absorption. The quantity of heat dissipated and absorbed by the junction is defined as follows:

$$Q_{\text{Peltier}} = N\pi_{\text{pn}}I = N(\pi_{\text{p}} - \pi_{\text{n}})I \tag{2}$$

where π_{p} and π_{n} are the Peltier coefficient of P-and N-type materials; π_{pn} is the Peltier coefficient of the TC, and I is the electrical current of the circuit.

The Thomson effect is observed when heat dissipation, absorption, or emission occurs in a conductor with a temperature gradient. The quantity of heat dissipation and absorption is governed by the conductor's temperature gradient and current density. The quantity of heat created per unit volume when a current density J travels through a conductor is as follows:

$$Q_{\text{Thomson}} = \rho J^2 - \mu \text{J}\frac{dT}{dx} \tag{3}$$

where ρ is the electrical resistivity of the material, dT/dx is the temperature gradient along the conductor, and μ is the Thomson coefficient with the same units as the Seebeck coefficient.

These three effects work together to create the total thermoelectric phenomenon. These three thermoelectric coefficients are correlated as follows:

$$\pi = \alpha T \tag{4}$$

$$\mu = T\frac{d\alpha}{dT} \tag{5}$$

Eq. 2 can be re-expressed by Eq. 4 (Eq. 6). In addition to the Peltier effect, current I induces the Joule effect due to the internal resistance R. The amount of heat generated by the Joule effect is expressed by Eq. 7.

$$Q_{\text{Peltier}} = N\alpha_{PN}TI \tag{6}$$

$$Q_{\text{Joule}} = I^2\text{R} \tag{7}$$

The basic characteristics of the thermoelectric element can be expressed in terms of the temperature distribution in the element being one-dimensional, the temperature of the high and low temperature sections, and the element's current or voltage. It is possible to represent the quantity of heat transmitted from a heat source to a high temperature section, or from a low temperature section to heat storage as follows:

$$Q_{\text{h}} = N\alpha T_{\text{h}}I + \frac{(T_{\text{h}} - T_{\text{c}})}{R_{TEG}} - \frac{I^2\text{R}_{\text{h}}}{2} \tag{8}$$

$$Q_{\text{c}} = N\alpha T_{\text{c}}I + \frac{(T_{\text{h}} - T_{\text{c}})}{R_{TEG}} - \frac{I^2\text{R}_{\text{c}}}{2} \tag{9}$$

In Eqs. 8 and 9, the first term on the right is related to the Peltier effect, the second term is related to heat conduction, and the third term is related to the Joule effect. R_{h} is the thermal resistance between the heat source and the TEG surface of the hot side, whilst R_{c} is the thermal resistance between the heat source and the TEG surface of the cold side. $Q_{\text{h}}$and Qc can be replaced as follows:

$$Q_{\text{h}} = \frac{(T_1 - T_{\text{h}})}{R_{\text{h}}} \tag{10}$$

$$Q_{\text{c}} = \frac{(T_{\text{c}} - T_2)}{R_{\text{c}}} \tag{11}$$

Fig. 5 shows the concept of the TEG. R_{L} and R_{TEG} denote the external and internal resistances, respectively. The power output P of the TEG is expressed using Eq. 12. The maximum power output P_{max} where the external and internal resistances coincide is expressed as Eq. 13.

$$P = (N\alpha_{\text{pn}}\Delta T + IR)I = V_{out}^2 I = V_{out}^2\frac{R_{\text{L}}}{(R_{\text{TEG}} + R_{\text{L}})^2} \tag{12}$$

$$P_{\text{max}} = \frac{V_{out}^2}{4R_{\text{TEG}}} \tag{13}$$

$$R_{\text{TEG}} = N\left(\frac{\rho_{\text{p}}L_{\text{p}}}{\alpha_{\text{p}}} + \frac{\rho_{\text{n}}L_{\text{n}}}{\alpha_{\text{n}}} + 2\frac{\rho_{\text{con}}L_{\text{con}}}{\alpha_{\text{con}}}\right) \tag{14}$$

where ρ_{p}, ρ_{n}, and ρ_{con} are the electrical resistivity of the P- and N-type leg materials and the conductor, respectively; L_{p} and L_{n} are each of the thermocouple leg lengths crossed by the heat flow; L_{con} is the conductor length, and R_{L} and R_{TEG} are the respective electrical resistances of the external and internal TEGs.

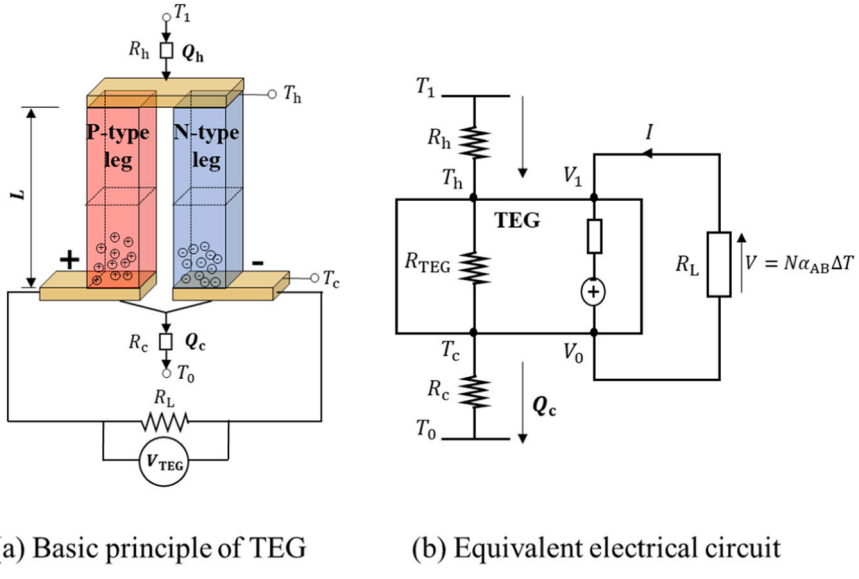

Fig. 5. Concepts of thermoelectric generator: (a) Basic principle of TEG, (b) Equivalent electrical circuit.

3.2. Efficiency of thermoelectric materials

The conversion efficiency of a thermoelectric element, stated as the zT value, is defined as the material's figure of merit and is determined only by the material's temperature and electrical and thermal properties. It is apparent that the efficiency of a TEG rises with the zT value. Therefore, in order to boost efficiency, the zT value of the thermoelectric material should be maximized. The electrical conductivity, Seebeck coefficient, and thermal conductivity of the thermoelectric material all contribute to the zT value, which rises in proportion to the operating temperature.

$$zT = \frac{\alpha^2 \sigma}{\lambda} T \tag{15}$$

TEGs can convert low-level heat sources into electricity. A TEG's conversion efficiency is defined by the ratio of output power to heat, whilst a TEG's COP can be expressed as the ratio of heat and output power, as follows:

$$\eta_{\mathrm{TEG}} = \frac{P_{\mathrm{out}}}{\mathrm{Q}} = \eta_c \frac{\sqrt{1+\mathrm{zT}}-1}{\sqrt{1+\mathrm{zT}}+(\mathrm{T}_c+273.15)/(\mathrm{T}_{\mathrm{h}}+273.15)} \tag{16}$$

$$\mathrm{COP} = \frac{Q}{\mathrm{P}_{\mathrm{out}}} \tag{17}$$

where, $\eta_c = \frac{(\mathrm{T_h}-\mathrm{T_c})}{\mathrm{T_h}+273.15}$ is Carnot's efficiency.

According to the obtained conversion efficiency, the electric power produced from the TEG application is calculated in Eq. (18). Here, the electric power refers to the TEG application, having an area of 0.1 m^2, proposed in this study. It is determined by the temperatures on both the hot and cold sides, which arise from the inlet and outlet temperatures of each component, and also by the conversion efficiency

$$P_{\mathrm{TEG}} = \eta_{\mathrm{TEG}} \times A_{\mathrm{TEG}} \times \frac{T_{\mathrm{h}} - T_{\mathrm{c}}}{R_{\mathrm{TEG}}} \tag{18}$$

The maximum zT value is an essential parameter that defines the TEG's output power. A commercially available thermoelectric element has a zT value of approximately 1, with a conversion efficiency of 10–15%. However, TEG applications requiring zT values of 3–4 are necessary for a wide range of commercial applications (Kumar and Singh, 2021).

3.3. Heat and electric generation of PVT and GHE

Photovoltaic (PV) power generation is a popular technology since it allows electricity generation by conversion from solar energy, whilst also having straightforward installation. However, high ambient temperatures and excessive panel temperatures caused by solar radiation can impair the efficiency of electricity generation. To compensate for these drawbacks, the PVT includes a heat exchanger in the bottom half of the solar panel in order to reduce the overall temperature and to use the heat-exchanged fluid for heating and cooling. Depending on the operating temperature, the fluid collected from the PVT is either immediately stored in the heat storage tank (HST) and utilized for heating, or in the solar storage tank (SST) and used as a heat source for the heat pump in this study. Furthermore, if the water outlet temperature of the GHE is less than that of the SST by more than 5 °C, the heat pump's water outlet temperature circulates through the GHE and returns to the SST to recover the ground temperature.

The PVT's electricity generation can be determined using the efficiency of the PV cell, temperature, and solar radiation, and is calculated as follows:

$$P_{\mathrm{PVT}} = (\tau a)_{\mathrm{n}} IAM \bullet G \bullet A_{\mathrm{PVT}} \bullet \eta_{\mathrm{PVT}} \tag{19}$$

where P_{PVT} is the power generation of the PVT; τa is the transmittance–absorbance production of the PVT; *IAM* is the incidence angle modifier; G is the beam and diffuse radiation incident on the PV cell surface; A_{PVT} is the area of PVT, and η_{PVT} is the power efficiency of the PV cell. The power efficiency of the PV cell is given as:

$$\eta_{\mathrm{PVT}} = \eta_{\mathrm{nominal}} \bullet X_{\mathrm{celltemp}} \bullet X_{\mathrm{radiation}} \tag{20}$$

where X_{celltemp} is the multiplier for the power efficiency as a function of the PV cell temperature, and $X_{\mathrm{radiation}}$ is the multiplier for the power efficiency as a function of the incident radiation.

The heat exchanger installed on the back of the solar panel lowers the PVT temperature via the flow of the working fluid and can be used as a heat source for the heat pump via the HST or SST. The temperature of the fluid released from the PVT's heat exchanger is calculated using Eq. 20, and the heat exchange rate (HER) using Eq. 21:

$$T_{\mathrm{PVT,out}} = \left(\mathrm{T}_{\mathrm{PVT,in}} + \frac{\varepsilon}{\kappa}\right) \exp\left(L \bullet \frac{N_{tube}}{\dot{m} C_p} \bullet \frac{\kappa}{\theta}\right) - \frac{\varepsilon}{\kappa} \tag{21}$$

$$Q_{\mathrm{PVT}} = \dot{m} C_p \left(T_{\mathrm{PVT,out}} - T_{\mathrm{PVT,in}}\right) \tag{22}$$

where C_p is volumetric heat capacity, $\dot{m}$ is flow rate, ε is emissivity on the PVT surface, and θ is angle of incidence [°].

The geothermal heat pump system uses the consistent subterranean temperature of 10–20 °C per year and is approximately 20–50% more efficient than the air heat source heat pump. The geothermal heat pump's performance may be represented as the relationship between the circulating water temperature $T_{\mathrm{GHE,out}}$ from the heat source to the heat pump, the water supply temperature $T_{\mathrm{building,in}}$ from the heat pump to the room, and the building load Q_{building}. It can also be estimated using the building load to heat pump power consumption ratio (Eq. 22). Eq. 23 may also be used to derive $T_{\mathrm{GHE,out}}$.

$$\mathrm{COP}_{\mathrm{heating}} = f\left(Q_{\mathrm{building}}, T_{\mathrm{GHE,out}}, T_{\mathrm{building,in}}\right) = \frac{Q_{\mathrm{building}}}{P_{\mathrm{HP}}} = \frac{Q_{\mathrm{GHE}} + P_{\mathrm{HP}}}{P_{\mathrm{HP}}} \tag{23}$$

$$T_{\mathrm{GHE,out}} = T_{\mathrm{GHE,in}} - \frac{Q_{\mathrm{GHE}}}{\dot{m} C_p} \tag{24}$$

The thermal resistance of the pipes can be indicated as a series sum of the resistances. The total pipe resistances are calculated by the sum of the pipe resistance and fluid resistance. The conductive resistance of the pipe is derived from the steady-state heat conduction for the radial system. The heat convection of the fluid in the pipe is calculated by considering the flow rate and viscosity of the fluid, the diameter and shapes of the pipe, etc.

$$R_{\mathrm{pipe}} = R_{\mathrm{p,con}} + R_{\mathrm{p,f}} \tag{25}$$

$$R_{\mathrm{p,con}} = \frac{1}{2\pi\lambda_{\mathrm{p}}} \ln\left(\frac{r_{p,o}}{r_{p,i}}\right) \tag{26}$$

$$R_{\mathrm{p,f}} = \frac{1}{2\pi r_{\mathrm{p,in}} h_{\mathrm{f}}} \tag{27}$$

Convective heat transfer efficiency at the inner surface of the pipe, h_{f}, is calculated by the Nusselt number (*Nu*). *Nu* is a function of the roughness of the surface and the flow velocity.

$$h_{\mathrm{f}} = \frac{Nu \lambda_{\mathrm{f}}}{2 r_{\mathrm{p,in}}} \tag{28}$$

$$Nu = \frac{(F/8)(\mathrm{Re}-1000)\mathrm{Pr}}{1+12.7(F/8)^{1/2}(\mathrm{Pr}^{2/3}-1)} \tag{29}$$

The Nusselt number is valid under the conditions of the Reynolds number $(3 \times 10^3 \leq \mathrm{Re} \leq 5 \times 10^6)$ and the Prandtl number $(0.5 \leq \mathrm{Pr} \leq 2000)$.

$$\mathrm{Re} = \frac{\rho_f v_f d_{p,in}}{\mu_f} = v_f d_{p,in} \Big/ \upsilon_f \tag{30}$$

$$\mathrm{Pr} = \mu_f c_f / \lambda_f \tag{31}$$

The friction factor, F, can be obtained from Eq. 30.

$$F = (0.79\ln(\mathrm{Re}) - 1.64)^{-2} \tag{32}$$

The temperature of the fluid flowing through the pipe is calculated under conditions where the pipe is insulated as follows;

$$q = c_f \rho_f \dot{m}(T_{f,h} - T_{f,c}) \tag{33}$$

$$q = \frac{1}{R_{pipe}} A(T_{f,h} - T_{TEG}) \tag{34}$$

$$T_{f,c} = T_{f,h} - \frac{c_f \rho_f \dot{m}}{R_{pipe}} \quad A(T_{f,h} - T_{TEG}) \tag{35}$$

4. System performance and temperature range in active systems

4.1. Operating temperature in each unit

Fig. 6 shows the inlet and outlet temperatures of the PVT, and its temperature difference. The circulating pump of PVT to obtain the thermal energy works under four conditions: 1) If the PVT outlet temperature is lower than the SST temperature, it remains inactive. 2) When the PVT outlet temperature is higher than the SST temperature but lower than the GHE temperature, it functions to store heat in the SST. 3) If the PVT outlet temperature passes over the GHE outlet temperature but remains lower than the HST temperature, it serves as a heat source for the heat pump. Lastly, when the PVT outlet temperature exceeds that of the HST, it operates to accumulate heat in the HST. Three hours after sunrise, the PVT, which had been heated, exceeded the outlet temperature of the SST. The excess heat generated by the PVT was then employed to elevate the temperature of the SST. From noon onwards (12:00 PM), the outlet temperature of the PVT water rose to around 27 °C and then gradually declined (Fig. 5b). Nevertheless, the impact of the external temperature during the heating period prevented the PVT outlet temperature from surpassing 42 °C, and as a result, the heating function through thermal storage in the Heat Storage Tank (HST) remained inactive.

Fig. 7 shows the inlet and outlet temperatures, as well as the temperature difference, of the ground heat exchanger (GHE) in operation. When $T_{GHE,out}$ exceeded $T_{SST,out}$, the circulation pump of GHE was activated, and when $T_{SST,out}$ exceeded $T_{GHE,out}$ by 5 °C, $T_{SST,out}$ circulated through the heat exchanger. In general, heat exchange with the GHE reduced ground temperature and degraded system performance, whereas the GHE in this study recovered ground temperature using the circulating water in the SST, thereby preventing performance degradation. During the operation period, $T_{GHE,out}$ was maintained at 14 ±25 °C, whilst the inlet-outlet temperature difference was in the range of 4–6 °C.

Fig. 8 shows the HST inlet and outlet temperatures as well as the temperature difference. $T_{HST,out}$ was calculated using the outlet temperature of HST set at 42 °C or higher for interior heating and the supply temperature set at 42–47 °C to maintain the indoor temperature of 22 °C. The average temperature difference between the inlet and outlet was approximately 3.9 °C. At 11:00–13:00, the flow rate was managed based on the low building load, and the temperature difference between inlet and outlet rose to approximately 6–12 °C.

4.2. System performance

Fig. 9 shows the PVT's electricity generation, which was calculated using global solar radiation data from Seoul, Korea, between November and March. The maximum solar radiation during the heating period was 899.7 W/m2, whilst the daily average solar radiation and electricity generation efficiency were 247.7 W/m2 and 14.1%, respectively. The daily average electricity generation for the applied PVT area of 19.9 m2 was 5.68 kWh, and power generation of approximately 1.6 kW was possible when maximum solar radiation was provided.

Fig. 10 shows each unit's heat exchange rate (HER). Under laboratory conditions, the heat exchange rate of the PVT was 30–50%, while the average period heat exchange rate was a relatively low 16.3%. This is because the average exterior temperature throughout the heating period was as low as 1.3 °C, indicating that heat loss to the external temperature was significant. Furthermore, the daily PVT heat exchange rate varied with global solar radiation, with the greatest and lowest daily average HERs determined to be 2.02 kW and 0.25 kW, respectively. The average HER throughout the period was 0.91 kW. The GHE's heat exchange rate maintained a relatively constant performance compared to the system operation in terms of preventing a drop in ground temperature (when $T_{SST,out} \geq T_{GHE,out} + 5$, $T_{SST,out}$ was circulated in the ground heat exchanger to recover the ground temperature). The average HER of the GHE during the period was 7.44 kW, whilst the maximum and minimum daily average HERs were determined to be 5.89 kW and 6.985 kW, respectively. Fig. 10 shows the COP of the heat pump during

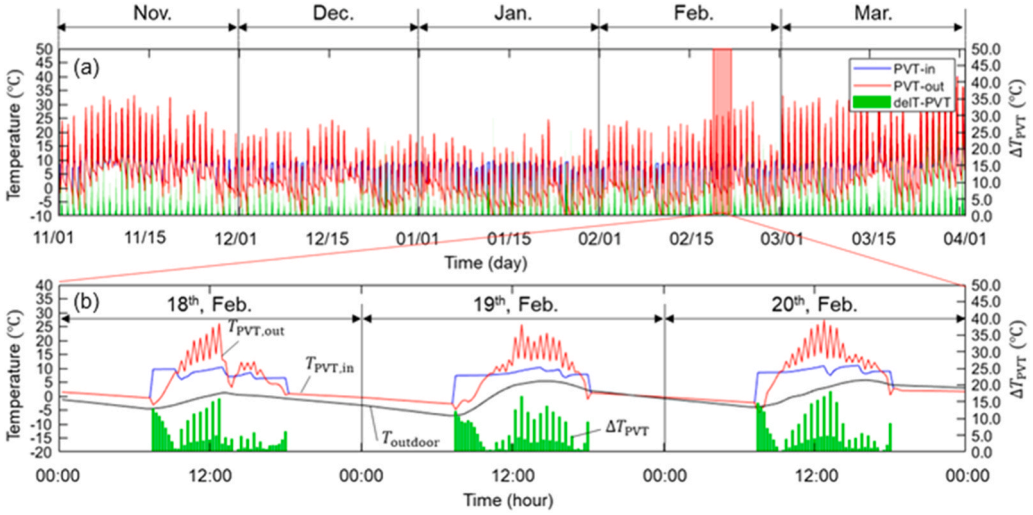

Fig. 6. Temperature change of PVT over time: (a) temperature change of PVT during heating period and (b) temperature change of PVT during representative heating days.

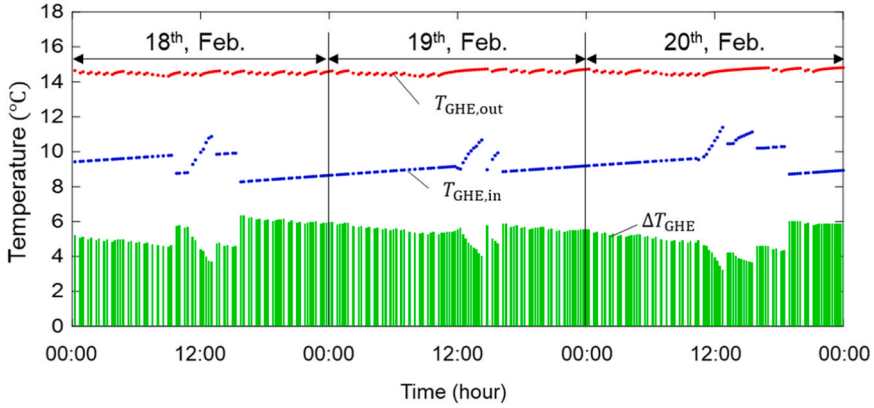

Fig. 7. Temperature change of GHX during representative heating days.

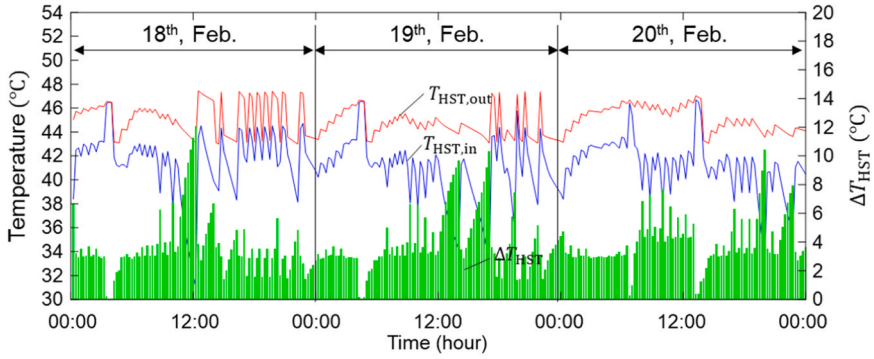

Fig. 8. Temperature change of HST during representative heating days.

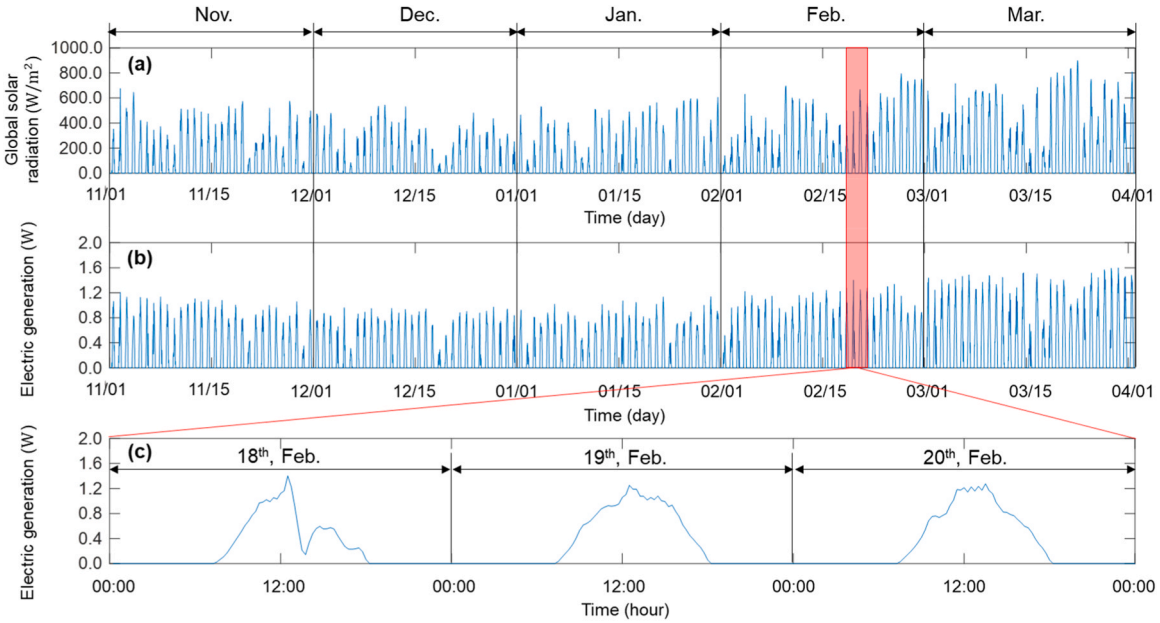

Fig. 9. Electric generation of PVT.

the heating period, which was maintained in the range of 3.07–3.91, with a monthly average COP of approximately 3.34. Fig. 11.

5. Feasibility study of TEG application

5.1. Electric power generation of TEG application

To assess the feasibility of the TEG applications proposed in this study, the electrical power generation of TEG produced in each unit was

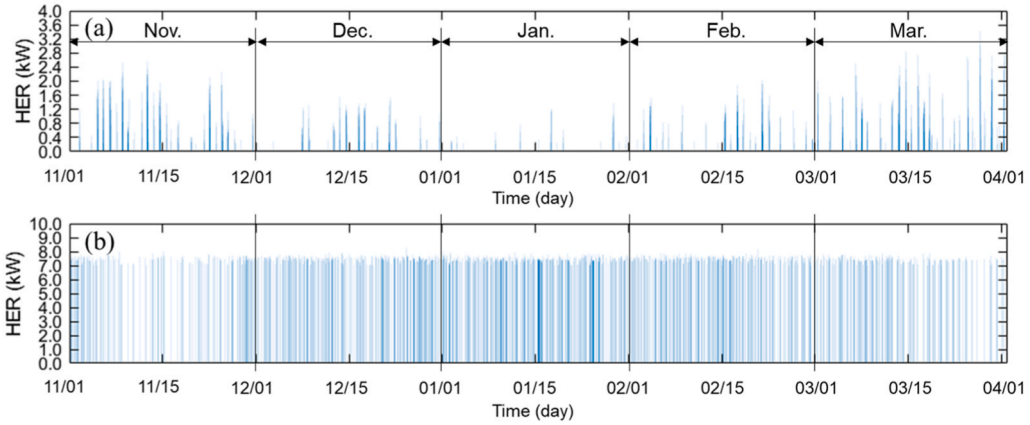

Fig. 10. Heat exchange rate in each object: (a) PVT and (b) GHX.

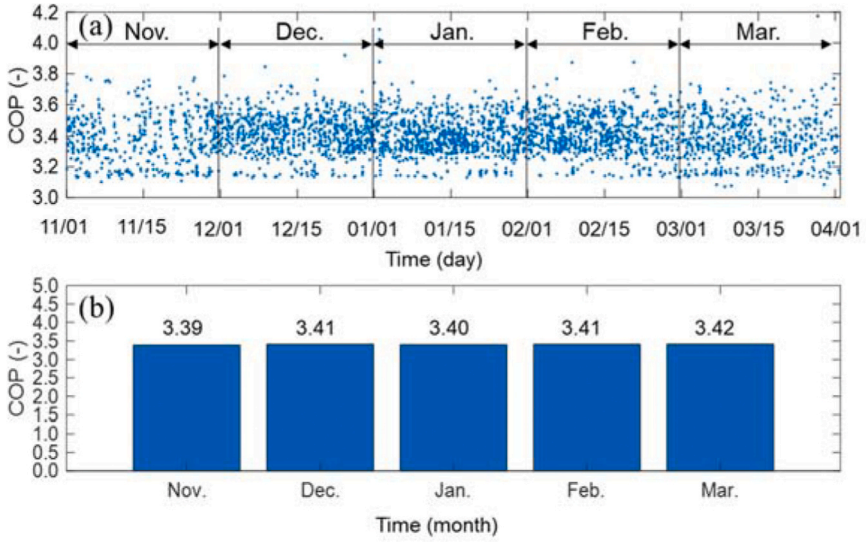

Fig. 11. COP of heat pump: (a) daily performance and (b) monthly average performance.

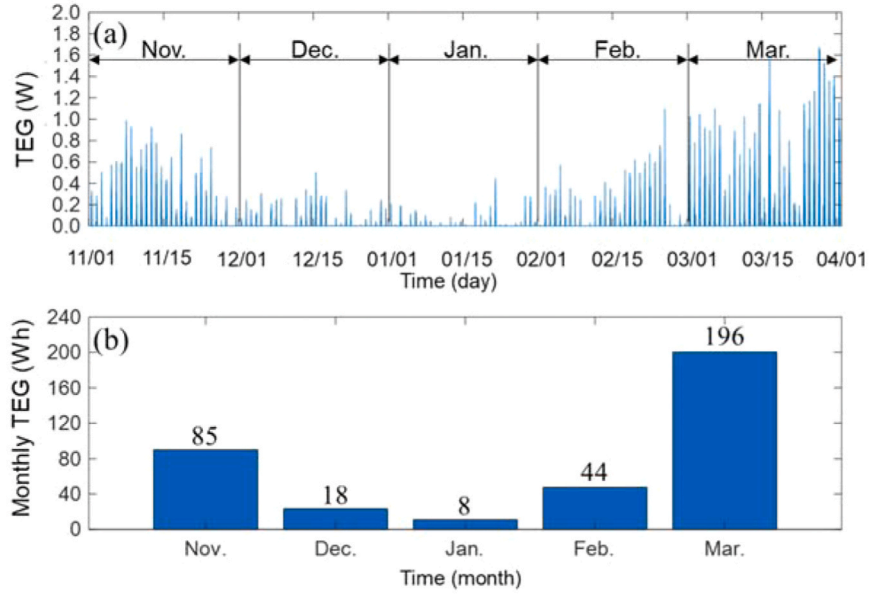

Fig. 12. TEG of PVT: (a) TEG of PVT over time and (b) monthly accumulated TEG.

calculated with a zT value of 1. Fig. 12 shows the electricity generation of the TEG applied to the PVT. Solar radiation and external temperature had a significant impact on the heat exchange rate of the PVT. As a result, during the coldest month of the year, January, the GHE was used to heat the house rather than the circulating water stored in the PVT. Thus, considerably less electricity generation was achieved in January compared to other months resulting from the limited number of operating days of the PVT and the absence of temperature differences between the inlet and outlet. However, the number of operating days of the PVT rose in March, resulting in the generation of approximately 196 Wh of electricity.

Fig. 13 shows the electricity generation of the TEG applied to the GHE during the representative heating period. In comparison with other units, the GHE could produce a constant power output while maintaining a relatively constant temperature difference of approximately 4–6 °C. In contrast to the PVT, the most electricity was generated in the month of January, when there were many operating days, and as a result, approximately 1389 Wh of electricity were obtained. When the external temperature was low, the GHE, which was relatively unaffected by external disturbances compared to the PVT, could generate a large amount of electricity.

Fig. 14 shows the electricity generation of the TEG applied to the HST during the representative heating period. The HST water outlet temperature ($T_{HST,out}$) was 42–47 °C, while the $T_{HST,in}$ temperature range fluctuated depending on heating demand. In particular, owing to the lower exterior temperature in January, the heat loss was significant, and the temperature of $T_{HST,in}$ recovered as the HST declined. The temperature difference of the HST rose, as did the electricity generated. The electricity generation during January was an estimated 1530 Wh, more than double that generated in November.

5.2. Potential of TEG application

Since the development of the TEG in 2000, the zT value, which remained in the 0.5 range, has been increased to approximately 2.5 as a result of advances in material science and nano-processing technology, although the zT value for TEG application suitable at ambient temperature has remained close to 1 (Polozine et al., 2014; Zhao and Tan, 2014; Recatala-Gomez et al., 2020). Nonetheless, it is anticipated that the development of nano-scale semiconductors would enable the achievement of a zT value that can allow the efficient use of TEGs for industrial application in the future. A TEG in this study was applied to each unit in an area of 0.1 m^2, and the quantity of electricity generated by the TEG throughout the heating time was 10.95 kWh when zT = 1. The quantity of energy generated with a zT value of 1 was sufficient to power one LED throughout the heating period (10 W, when used for 8 h a day).

In this study, the area of TEG necessary to accomplish a zero-energy building (ZEB) was estimated. The heat pump used 10413 kWh of electricity throughout the heating period, while the PVT produced 3432 kWh. Therefore, additional power of 6980 khW was needed to accomplish a ZEB, and the installation area of the TEG based on zT was computed for additional power generation. Here, the installation area for the TEG application corresponds to the length of the pipe. The TEG application is installed sequentially, starting from the heat sources (from the inlet and outlet of objects). Based on Eqs. 24–34, both the temperature change of the fluid as the TEG application increases and the consequent power output were calculated. When zT was 1, the required TGE installation space in each unit was 64.5 m^2.

6. Conclusion

A feasibility study was performed on the use of a TEG in each system unit for houses using a hybrid system. The highest electricity generation efficiency was obtained in the HST with a relatively large temperature difference and the long operating time among the units to which TEG was applied. The electricity produced by the TEG was determined to be 10.95 kWh when the planned TEG was applied to each unit individually. Furthermore, the additional electricity necessary to achieve a ZEB required a TEG application of 64.5 m^2 for each unit, based on a zT of 1.

This study performed a feasibility study on the application of TEG to the active system. The electricity generation of the TEG applied to the active system was relatively small, and a large area was needed to deliver additional power to the heat pump. However, the TEG showed sufficient applicability as a power source for data loggers and other sensors in a building system. Furthermore, we are confident that TEGs will be applied further, and subsequently achieve significant commercial success with the introduction of additional low-power devices and the continual increase in the zT value of thermoelectric materials.

TEGs transform heat into electrical energy using the Seebeck effect. Their efficiency depends on the merit of thermoelectric materials, the temperature gradient, and the balance between a heat source and a cool sink. Challenges arise from material degradation, mechanical stresses due to thermal cycling, elevated costs, and parasitic power losses. These issues can result in diminished performance and greater expenses compared to conventional power sources. To enhance the efficiency and lifespan of TEGs, researchers are delving into new thermoelectric materials with superior ZT values, innovating manufacturing techniques, and devising systems that curtail parasitic losses and thermal

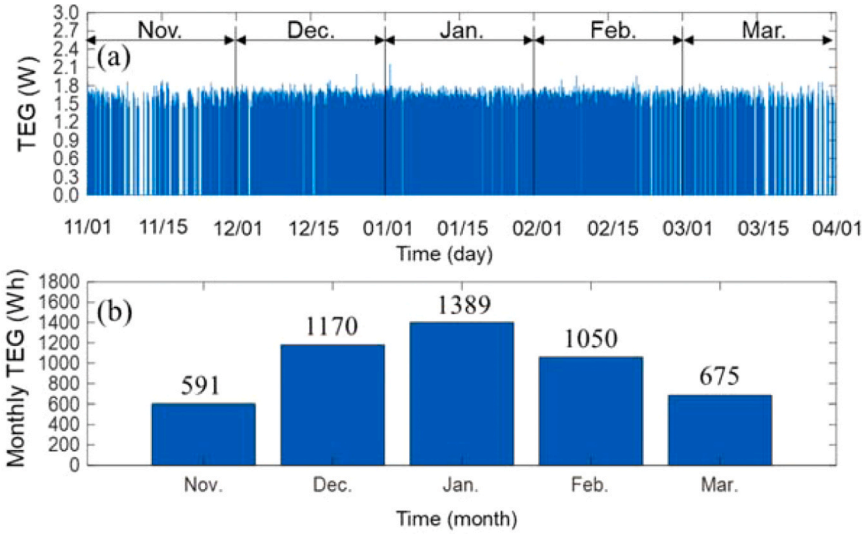

Fig. 13. TEG of GHE: (a) TEG of GHE over time and (b) monthly accumulated TEG.

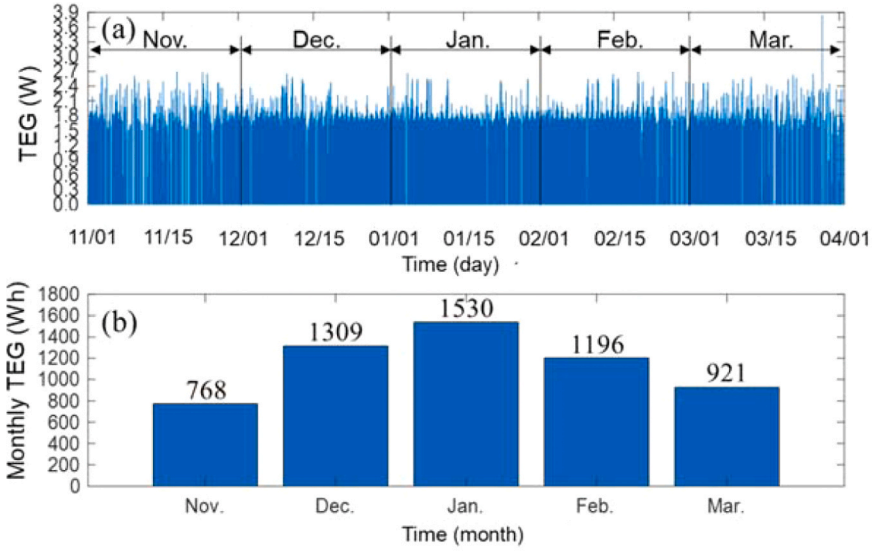

Fig. 14. TEG of HST: (a) TEG of PVT over time and (b) monthly accumulated TEG.

resistances. Further, incorporating TEG incentives into Life Cycle Cost and considering environmental policies and carbon emissions in Life Cycle Assessment (LCA) are imperative. In upcoming studies, our research team intends to validate proposed applications via empirical experiments and evaluate the LCA for TEG applications.

CRediT authorship contribution statement

Hobyung Chae: Conceptualization, Investigation, Methodology, Formal analysis, Writing – original draft. **Sangmu Bae**: Data curation. **Jae-Weon Jeong**: Formal analysis. **Yujin Nam**: Project administration, Writing – review & editing.

Declaration of Competing Interest

The authors declare that they have no known competing financial interests or personal relationships that could have appeared to influence the work reported in this paper.

Data availability

Data will be made available on request.

Acknowledgement

This research was supported by Basic Science Research Program through the National Research Foundation of Korea (NRF) funded by the Ministry of Education (NRF-2022R1A4A1026503 and No. 2022R1A6A3A01087099) and the Korea government (MSIT) (No.2021R1A2C2014259).

References

A. Proto L. Peter M. Cerny M. Penhaker D. Bibbo S. Conforto M. Schmid Human body energy harvesting solutions for wearable technologies, 2018 IEEE 20th Int. Conf. e-Health Networking Appl. Serv. Heal. 2018 2018 doi: 10.1109/HealthCom.2018.8531189.

Ahmed, A., Ge, T., Peng, J., Yan, W.C., Tee, B.T., You, S., 2022. Assessment of the renewable energy generation towards net-zero energy buildings: a review. Energy Build. 256, 111755 https://doi.org/10.1016/j.enbuild.2021.111755.

Bae, S., Nam, Y., 2021. Comparison between experiment and simulation for the development of a Tri-generation system using photovoltaic-thermal and ground source heat pump. Energy Build. 231, 110623 https://doi.org/10.1016/j.enbuild.2020.110623.

Boulanger, C., 2010. Thermoelectric material electroplating: a historical review. J. Electron. Mater. 39, 1818–1827. https://doi.org/10.1007/s11664-010-1079-6.

Byon, Y.S., Jeong, J.W., 2020. Annual energy harvesting performance of a phase change material-integrated thermoelectric power generation block in building walls. Energy Build. 228, 110470 https://doi.org/10.1016/j.enbuild.2020.110470.

Campagna, L.M., Fiorito, F., 2022. On the impact of climate change on building energy consumptions: a meta-analysis. Energies 15. https://doi.org/10.3390/en15010354.

Chung, D., Hogan, T.P., Rocci-Lane, M., Brazis, P., Ireland, J.R., Kannewurf, C.R., Bastea, M., Uher, C., Kanatzidis, M.G., 2004. A new thermoelectric material: CsBi 4 Te 6 S. J. Am. Chem. Soc. 126, 6414–6428.

Gherasim, I., Taws, M., Galanis, N., Nguyen, C.T., 2011. Heat transfer and fluid flow in a plate heat exchanger part I. Experimental investigation. Int. J. Therm. Sci. 50, 1492–1498. https://doi.org/10.1016/j.ijthermalsci.2011.03.018.

Guan, M., Wang, K., Xu, D., Liao, W.H., 2017. Design and experimental investigation of a low-voltage thermoelectric energy harvesting system for wireless sensor nodes. Energy Convers. Manag. 138, 30–37. https://doi.org/10.1016/j.enconman.2017.01.049.

Hamilton, I., Rapf, O., 2020. E2020 global status report for buildings and construction: towards a zero-emissions, efficient and resilient buildings and contruction sector. Glob. Alliance Build. Constr. 1–7.

Iezzi, B., Ankireddy, K., Twiddy, J., Losego, M.D., Jur, J.S., 2017. Printed, metallic thermoelectric generators integrated with pipe insulation for powering wireless sensors. Appl. Energy 208, 758–765. https://doi.org/10.1016/j.apenergy.2017.09.073.

Joung, T.H., Kang, S.G., Lee, J.K., Ahn, J., 2020. The IMO initial strategy for reducing Greenhouse Gas(GHG) emissions, and its follow-up actions towards 2050. J. Int. Marit. Saf. Environ. Aff. Shipp. 4, 1–7. https://doi.org/10.1080/25725084.2019.1707938.

Khan, M.S., Bai, Y., Chen, Z., Huang, Q., Zou, X., 2020a. Conceptual design and numerical assessment of compact heat exchanger for lead-based reactor. Prog. Nucl. Energy 124, 103348. https://doi.org/10.1016/j.pnucene.2020.103348.

Khan, M.S., Bai, Y., Huang, Q., Xu, C., Sun, L., Zou, X., Wang, L., 2020b. Conceptual design and optimization of power generation system for lead-based reactor. Appl. Therm. Eng. 168, 114714 https://doi.org/10.1016/j.applthermaleng.2019.114714.

Khan, T.S., Khan, M.S., Chyu, M.C., Ayub, Z.H., 2010. Experimental investigation of single phase convective heat transfer coefficient in a corrugated plate heat exchanger for multiple plate configurations. Appl. Therm. Eng. 30, 1058–1065. https://doi.org/10.1016/j.applthermaleng.2010.01.021.

Kim, Y.J., Gu, H.M., Kim, C.S., Choi, H., Lee, G., Kim, S., Yi, K.K., Lee, S.G., Cho, B.J., 2018. High-performance self-powered wireless sensor node driven by a flexible thermoelectric generator. Energy 162, 526–533. https://doi.org/10.1016/j.energy.2018.08.064.

Ko, J., Jeong, J.W., 2021. Annual performance evaluation of thermoelectric generator-assisted building-integrated photovoltaic system with phase change material. Renew. Sustain. Energy Rev. 145, 111085 https://doi.org/10.1016/j.rser.2021.111085.

Kumar, R., Singh, R., 2021. Thermoelectricity and Advanced Thermoelectric Materials. Elsevier,.

Li, J., Wang, Y., Yang, X., Kang, H., Cao, Z., Jiang, X., Chen, Z., Guo, E., Wang, T., 2022. Processing bulk insulating CaTiO3 into a high-performance thermoelectric material. Chem. Eng. J. 428, 131121 https://doi.org/10.1016/j.cej.2021.131121.

Liu, C., Pan, X., Zheng, X., Yan, Y., Li, W., 2016. An experimental study of a novel prototype for two-stage thermoelectric generator from vehicle exhaust. J. Energy Inst. 89, 271–281. https://doi.org/10.1016/j.joei.2015.01.019.

Liu, K., Liu, Y., Xu, Z., Zhang, Z., Yuan, Z., Guo, X., Jin, Z., Tang, X., 2017. Experimental prototype and simulation optimization of micro-radial milliwatt-power radioisotope thermoelectric generator. Appl. Therm. Eng. 125, 425–431. https://doi.org/10.1016/j.applthermaleng.2017.07.022.

Liu, K., Tang, X., Liu, Y., Yuan, Z., Li, J., Xu, Z., Zhang, Z., Chen, W., 2018. High-performance and integrated design of thermoelectric generator based on concentric filament architecture. J. Power Sources 393, 161–168. https://doi.org/10.1016/j.jpowsour.2018.05.018.

Lu, Y., Wang, Y., Zhu, L., Wang, Q., 2010. Enhanced performance of heat recovery ventilator by airflow-induced film vibration (HRV performance enhanced by FIV). Int. J. Therm. Sci. 49, 2037–2041. https://doi.org/10.1016/j.ijthermalsci.2010.06.001.

Marszal, A.J., Heiselberg, P., Bourrelle, J.S., Musall, E., Voss, K., Sartori, I., Napolitano, A., 2011. Zero energy building - a review of definitions and calculation methodologies. Energy Build. 43, 971–979. https://doi.org/10.1016/j.enbuild.2010.12.022.

Matiko, J.W., Grabham, N.J., Beeby, S.P., Tudor, M.J., 2014. Review of the application of energy harvesting in buildings. Meas. Sci. Technol. 25 https://doi.org/10.1088/0957-0233/25/1/012002.

Mavromatidis, G., Orehounig, K., Richner, P., Carmeliet, J., 2016. A strategy for reducing CO_2 emissions from buildings with the Kaya identity - a Swiss energy system analysis and a case study. Energy Policy 88, 343–354. https://doi.org/10.1016/j.enpol.2015.10.037.

Nasif, M., Al-Waked, R., Morrison, G., Behnia, M., 2010. Membrane heat exchanger in HVAC energy recovery systems, systems energy analysis. Energy Build. 42, 1833–1840. https://doi.org/10.1016/j.enbuild.2010.05.020.

Omrany, H., Chang, R., Soebarto, V., Zhang, Y., Ghaffarianhoseini, A., Zuo, J., 2022. A bibliometric review of net zero energy building research 1995–2022. Energy Build. 262 https://doi.org/10.1016/j.enbuild.2022.111996.

Polozine, A., Sirotinskaya, S., Schaeffer, L., 2014. History of development of thermoelectric materials for electric power generation and criteria of their quality. Mater. Res. 17, 1260–1267. https://doi.org/10.1590/1516-1439.272214.

Recatala-Gomez, J., Suwardi, A., Nandhakumar, I., Abutaha, A., Hippalgaonkar, K., 2020. Toward accelerated thermoelectric materials and process discovery. ACS Appl. Energy Mater. 3, 2240–2257. https://doi.org/10.1021/acsaem.9b02222.

Sammeta, H., Ponnusamy, K., Majid, M.A., Dheenathayalan, K., 2011. Effectiveness charts for counter flow corrugated plate heat exchanger. Simul. Model. Pract. Theory 19, 777–784. https://doi.org/10.1016/j.simpat.2010.10.012.

Song, J., Kim, C., 2022. A study on strategies of public R & D to achieve national carbon neutrality: focusing on the Implications of the Republic of Korea. Asian J. Innov. Policy 1–29.

Thielen, M., Sigrist, L., Magno, M., Hierold, C., Benini, L., 2017. Human body heat for powering wearable devices: from thermal energy to application. Energy Convers. Manag. 131, 44–54. https://doi.org/10.1016/j.enconman.2016.11.005.

Vasiliev, M., Nur-E-Alam, M., Alameh, K., 2019. Recent developments in solar energy-harvesting technologies for building integration and distributed energy generation. Energies 12. https://doi.org/10.3390/en12061080.

Wang, W., Cionca, V., Wang, N., Hayes, M., O'Flynn, B., O'Mathuna, C., 2013. Thermoelectric energy harvesting for building energy management wireless sensor networks. Int. J. Distrib. Sens. Netw. 2013 https://doi.org/10.1155/2013/232438.

Zhang, Y., Cleary, M., Wang, X., Kempf, N., Schoensee, L., Yang, J., Joshi, G., Meda, L., 2015. High-temperature and high-power-density nanostructured thermoelectric generator for automotive waste heat recovery. Energy Convers. Manag. 105, 946–950. https://doi.org/10.1016/j.enconman.2015.08.051.

Zhao, D., Tan, G., 2014. A review of thermoelectric cooling: materials, modeling and applications. Appl. Therm. Eng. 66, 15–24. https://doi.org/10.1016/j.applthermaleng.2014.01.074.

Zhao, L.D., Chang, C., Tan, G., Kanatzidis, M.G., 2016. SnSe: a remarkable new thermoelectric material. Energy Environ. Sci. 9, 3044–3060. https://doi.org/10.1039/c6ee01755j.